

Article

A Novel Process to Produce Ti Parts from Powder Metallurgy with Advanced Properties for Aeronautical Applications

Tamas Miko ^{1,*}, Daniel Petho ¹, Greta Gergely ¹ , Dionysios Markatos ² and Zoltan Gacsi ¹

¹ Institute of Physical Metallurgy, Metalforming and Nanotechnology, University of Miskolc, 3515 Miskolc, Hungary

² Laboratory of Technology & Strength of Materials (LTSM), Department of Mechanical Engineering and Aeronautics, University of Patras, 26504 Patras, Greece

* Correspondence: femmiko@uni-miskolc.hu

Abstract: Titanium and its alloys have excellent corrosion resistance, heat, and fatigue tolerance, and their strength-to-weight ratio is one of the highest among metals. This combination of properties makes them ideal for aerospace applications; however, high manufacturing costs hinder their widespread use compared to other metals such as aluminum alloys and steels. Powder metallurgy (PM) is a greener and more cost and energy-efficient method for the production of near-net-shape parts compared to traditional ingot metallurgy, especially for titanium parts. In addition, it allows us to synthesize special microstructures, which result in outstanding mechanical properties without the need for alloying elements. The most commonly used Ti alloy is the Ti6Al4V grade 5. This workhorse alloy ensures outstanding mechanical properties, demonstrating a strength which is at least twice that of commercially pure titanium (CP-Ti) grade 2 and comparable to the strength of hardened stainless steels. In the present research, different mixtures of both milled and unmilled Cp-Ti grade 2 powder were utilized using the PM method, aiming to synthesize samples with high mechanical properties comparable to those of high-strength alloys such as Ti6Al4V. The results showed that the fine nanoparticles significantly enhanced the strength of the material, while in several cases the material exceeded the values of the Ti6Al4V alloy. The produced sample exhibited a maximum compressive yield strength (1492 MPa), contained 10 wt.% of fine (milled) particles (average particle size: 3 μm) and was sintered at 900 °C for one hour.

Keywords: titanium; powder metallurgy; aerospace; dual scale microstructure



Citation: Miko, T.; Petho, D.; Gergely, G.; Markatos, D.; Gacsi, Z. A Novel Process to Produce Ti Parts from Powder Metallurgy with Advanced Properties for Aeronautical Applications. *Aerospace* **2023**, *10*, 332. <https://doi.org/10.3390/aerospace10040332>

Academic Editors: Spiros Pantelakis, Andreas Strohmayer and Jordi Pons i Prats

Received: 28 February 2023
Revised: 16 March 2023
Accepted: 21 March 2023
Published: 27 March 2023



Copyright: © 2023 by the authors. Licensee MDPI, Basel, Switzerland. This article is an open access article distributed under the terms and conditions of the Creative Commons Attribution (CC BY) license (<https://creativecommons.org/licenses/by/4.0/>).

1. Introduction

Titanium and its alloys have a significant role in the aerospace industry. Demonstrating a density of 4.5 g/cm³, titanium alloys weigh about half as much as steel or Ni-based super alloys, resulting in superior mechanical properties to the latter, while their exceptional corrosion resistance makes them excellent candidates for use in the aviation and aerospace sectors [1]. Currently, this metal and its alloys account for 14% of the total weight of modern aircrafts [2,3]. For non-structural applications in which corrosion resistance, good formability and low weight are the main requirements (e.g., welded pipes and ducts, bolts, seat rails, water supply systems for galleys and sanitary, etc.), Cp-Ti is generally used. However, there are several application areas wherein high strength is important as well. Airframe joints, engine parts (e.g., fan blades, fan case, shaft, compressor) and landing gears require the use of high strength Ti alloys [4,5]. For these purposes, the Ti6Al4V is the most widely used alloy. Titanium-based alloys have the highest tensile strength/density ratio among the metals [6]. Unlike aluminum alloys, Titanium can preserve its strength at elevated (up to 600 °C) and cryogenic temperatures as well [7], which is favorable considering the temperature conditions affecting aircraft. Moreover, the ongoing focus on achieving closed-loop circularity in the aviation sector for the accomplishment of sustainability objectives [8]

can be supported by using recycled titanium alloys. Titanium alloys can be remelted and reprocessed into high purity ingots with lower energy requirements compared to virgin ones. In this context, specialized forging plants that recycle titanium from the aerospace sector are already functioning [9].

Yet, the biggest obstacle to the wider use of titanium is its price. Generally, the cost of the traditional production method is higher compared to other metals, such as steel or aluminum [10]. In addition, cold forming of thin titanium alloys is challenging due to their high yield strength (YS) and their significant strain hardening effect. Furthermore, they present low thermal conductivity, which increases the heat of the tools during machining, while their low Young's modulus causes a significant spring back during traditional processing [11]. Figure 1 shows the price per unit volume of some traditionally produced alloys used in the aerospace industry at different thicknesses [12]. Obviously, the Ti6Al4V alloy has the highest price compared to the unalloyed Ti grade 2, 17-4PH stainless steel and 7075 aluminum alloy. In the case of 7075 Al and Ti grade 2, the price does not increase significantly with decreasing thickness, due to their good formability. However, the specific prices of the 17-4PH stainless steel and the Ti6Al4V increase significantly with the thickness decrease. This is due to the resulting increase in hardness and strength. The latter can make the material more resistant to deformation during the cold forming, which in turn may require more energy to shape it. Additionally, thinner materials may require more precise and specialized equipment and processes to be shaped properly, which can also increase costs. Therefore, cold forming of these alloys is extremely difficult and energy demanding, especially for thinner sheets, something which increases processing costs significantly.

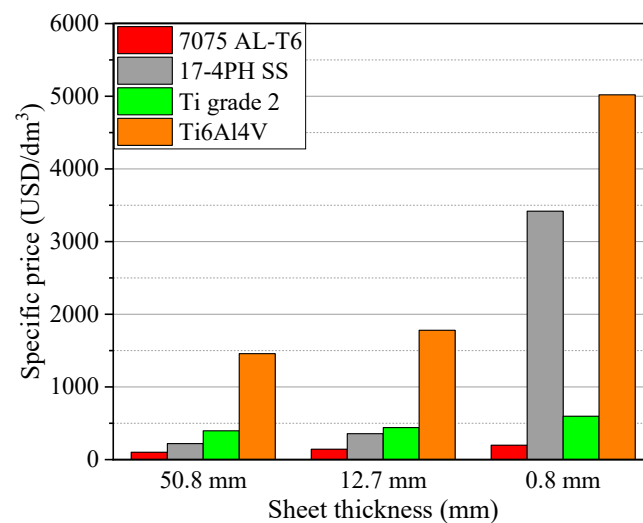


Figure 1. Specific price (USD/dm³) of different metal sheets (304 × 304 mm) at different thickness.

Furthermore, due to the low yield rate of the traditional Ti metallurgy, 82% of the initial Ti becomes scrap, e.g., in the case of F-22 fighter jet Ti parts [13]. In the above context, reduction of scrap material and consequent manufacturing costs, as well as increases in the mechanical properties of Cp-Ti and titanium alloys, represent the two main challenges of the research community [14]. Within this framework, the powder metallurgical (PM) approach can significantly increase the yield rate and thus reduce manufacturing costs, as it is suitable for the production of ready-to-use parts and components [10]. Among the PM processes, the traditional press and sinter process is the lowest cost method for converting metal powder into a near net shape part [15]. This method involves the cold pressing of the prepared powder into the desired shape in a die, then creating metallic bonding between the cold-welded powder particles via sintering at temperatures below the melting temperature. The productivity of this process is high, but the size and complexity of the cold pressed parts are limited due to technological reasons [16]; therefore, fan blades, cockpit window frames or hydraulic pipes cannot be produced this way. Cold isostatic

pressing (CIP) and hot isostatic pressing (HIP) can be alternative solutions to the press and sinter technique [17]; however, productivity is greatly decreased with these solutions.

However, the use of press and sinter technology has its limitations. The produced parts must be relatively small, as the required press force increases as the surface area increases. In addition, they must have an axisymmetric simple shape to be manufacturable with cold pressing tools. For example, fasteners (nuts, screws, clevis pins, washers) can be produced as a finished or semi-finished product this way. These products are traditionally made from rolled sheets and bars by chipping or punching, which results in a lot of scrap material. PM appears as a suitable method for the production of these small parts as it does not generate a considerable amount of scrap. This manufacturing process is particularly economical for expensive materials such as Ti and its alloys. From the observed high costs of small parts produced through conventional methods [18], it becomes clear that the PM technology could emerge as a potential cost-efficient method for the production of small parts such as thin washers, as such parts can be produced without generating any scrap material, thus saving on processing costs and energy.

The properties of PM products are significantly influenced by the size, morphology, and hardness of the initial powders. Duriagina et al. has investigated the effect of the size and morphology of the VT20 Ti alloy powders on the mechanical properties of coatings. The coatings deposited from the $-160 + 40 \mu\text{m}$ fraction showed an optimum ratio of strength and plasticity. Nonspherical VT20 titanium alloy powders are characterized by a finer structure than the coatings produced from spherical powders [19].

Although powders with spherical morphology are ideal for the additive manufacturing (AM) processes such as metal injection molding (MIM), they are not favorable for cold pressing due to the weak compressive bonds between the pressed powder particles. Powders with sponge-like particles ensure the highest green (i.e., not yet sintered part) strength [15] by promoting higher plastic deformation during cold compaction and better interlocking behavior compared to spherical powders [20]. The morphology of the Cp-Ti sponge results from the reduction of the Ti ore using the Kroll, Hunter or Armstrong method, which is the first main step of commercial titanium's production route [10]. The size of the coral-like spongy particles can be decreased to specified ranges by using a crushing or milling technique. This size reduction can easily be carried out after hydrogenating the powder. The resulting TiH_2 can be easily crushed to different particle sizes, ranging from $45 \mu\text{m}$ to $300 \mu\text{m}$. After this relatively inexpensive hydrogenation-dehydrogenation process (HDH), we obtain a powder with irregularly shaped particles with high purity [21]. Currently, the spherical Ti6Al4V powder is also produced from alloyed Kroll sponge; it is formed into a wrought product which is then reduced to powder by an atomization process (e.g., the plasma rotating electrode process (PREP)). The resulting spherical powder's cost is approximately 15–30 times of the cost of sponge Cp-Ti powder [14]. This feedstock ensures much higher sintered strength, but the cost could be higher than the production cost of the same wrought alloy. In the case of PM parts, the effect of porosity has an important role. In order to increase the relative density close to its theoretical maximum, most studies used high sintering temperatures and long sintering times, but in these cases, coarsening is a significant issue [22]. The applied value of the cold pressing has also an important role in the green density [23]. Decreasing the porosity from 35% to 5%, the strength (YS, UTS) and the elongation to fracture value increases by about 5 to 10 times, respectively [24]. The difference between the green density of the samples made of Ti6Al4V and the Cp-Ti is ~20% [20]. However, if we compare the tensile properties of the Cp-Ti and Ti6Al4V (Table 1), it can be stated that the strength (YS, UTS) of the sintered/wrought Ti6Al4V are double, while the elongation is half of the Cp-Ti's values [25].

Table 1. Tensile properties of Cp-Ti and Ti alloys.

Type	Production Method	Specification	Tensile YS (MPa)	UTS (MPa)	Tensile Strain (%)
CP-Ti (grade 2)	Metal Injection Molding (MIM)	ASTM F2989 MIM 2	360	420	17
	Wrought (forging stock)	EN 3451:2017	290	390	20
	Wrought (forging stock)	ISO 5832-2:1999	275	345	20
Ti6Al4V	Metal Injection Molding (MIM)	ASTM F2885 grade 5	680	780	10
	Additive Layer Manufacturing (ALM)	ASTM F2924	825	895	10
	Wrought (sheet or bar)	ISO 5832-3:2016	780	860	10
Ti-10V-2FE-3Al	Wrought hot rolled bars	EN 4685:2011	1110	1240	4

From the above table (Table 1), it is clear that the alloying elements play an important role on the strength of the alloys. There are several studies which have investigated the role of the different alloying elements on the strength of the titanium. By adding 42 wt.% Nb, the tensile yield strength increases to 675 MPa [26], and by adding 7 wt.% Fe, the tensile strength increases to 916 MPa [27]. The strength can even be increased more by adding ceramic reinforcement to Ti. Jeong et al. mixed pure titanium powder with TiB₂ and B₄C powder, then produced bulk samples using the press and sinter approach. The compressive yield strength of the in situ processed composites was higher than that of the Ti6Al4V alloy at ambient temperature. The highest compressive yield strength obtained was 1400 MPa [28]. The oxygen content has also an important role on the strength of the Ti. Chen et al. increased the oxygen content of the Cp-Ti up to 0.8 wt.%. using different PM methods. The highest tensile YS was measured around 900 MPa [20].

Besides the alloying and reinforcing elements, the role of the grain structure and the grain size are crucial as well, and this will be the focus of the present work. Nano-grained (NG) and ultrafine-grained (UFG) metals and alloys show significantly higher strength compared to coarse-grained metals [29]. However, with the increased strength, the deformability and the room temperature ductility significantly decrease as well, limiting the applicability. To tackle the latter issue, dual scale grain size can be considered. The big advantage of a dual scale grain size is that the coarse grains retain the toughness of the material, while the fine grains improve its strength [30]. This microstructure can be achieved by PM method. Sun et al. prepared non-milled and cryo-milled Ti6Al4V alloy by plasma-activated sintering. The highest hardness measured was 470 HV, and the highest compressive YS was 1706 MPa [31]. Li et al. made a Ti-Bi bimodal alloy by using high-energy ball-milled Ti-Bi and spark plasma sintering, achieving 1080 MPa tensile YS [32]. Attar et al. made in situ titanium–titanium boride composites using the mixture of fine TiB₂ and coarse CP-Ti powder. The solidification was carried out with the selective laser melting (SLM) method, achieving 1400 MPa compressive YS [33].

Based on the cited literature, the economically feasible production of Ti parts with satisfactory mechanical properties can still be further improved. In this study, Cp-Ti was considered the initial material, with the aim being to improve its performance using a dual-scale microstructure which was produced by mixing fine and coarse titanium grade-2 type powders through the PM process. The goal of the study was to produce a material with increased mechanical properties, to be considered as a potential substitute to commercially produced Ti alloys widely used in the aviation sector, such as the Ti6Al4V (grade5) alloy. To achieve the above, the cavities of Cp-Ti sponge powders were filled with fine nanoscale-milled Cp-Ti powder during the mixing process, which resulted in a special feedstock for the applied cold press and sinter process. The density, hardness, yield strength, compressive strength and strain were systematically investigated on the sintered parts. The results showed that the fine nanoparticles of the dual-scale grain have significantly enhanced the strength of the material, while in several cases, the corresponding strength exceeded the values of the Ti6Al4V alloy. The novelty of the work lies in the simplicity and inexpensiveness of the production route.

2. Experimental

The Ti powder used is a 99.4% purity Cp-Ti (grade 2) with nominal average particle size of 150 μm , produced by Alfa Aesar (product number: 10383), Kandel, Germany. The received (coded as “initial”) powder was used as coarse-grained Ti, and the fine-grained Ti was produced from the same powder by use of high-energy ball milling. The milling was carried out with a Pulverisette 5 high-energy planetary ball mill (Fritsch, Idar-Oberstein Germany) at room temperature for 20 h. In order to prevent excessive cold welding, alcohol was used as a process control agent (PCA). The milling was performed in Ar atmosphere using a 250 mL hardened steel vial and hardened steel balls of 8 mm diameter. The ball-to-powder (BPR) weight ratio and rotational speed were 30:1 and 200 rpm, respectively. The mixing of the initial and milled powders was also carried out with the same mill, but the milling parameters were changed to 10:1 BPR, 30 min and 100 rpm. Ethanol was not used in this case. During mixing, 2; 4; 6; 8 and 10 wt.% milled Ti was added to the initial Ti powder.

Instron 5982 (Norwood, MA, USA) equipment was used for the consolidation of the powders to green parts at ambient temperature. The mixed powders were placed in a hardened steel die between hardened steel punches to produce cylindrical specimens with a diameter of 8 mm and 8 mm height. Graphite 33 spray (Iffezheim, Germany) was used as lubricant on the die walls to decrease the friction, and during the cold uniaxial pressing, 1.6 GPa pressure was applied. The sintering of the green samples was carried out in an electric furnace (SF 16 type Three-Zone Split Tube Furnace, Norwood, MA, USA) in Ar 6.0 atmosphere (Siad Hungary, Miskolc, Hungary). Four different sintering temperatures were considered: 800, 850, 900 and 950 $^{\circ}\text{C}$. The heating and the cooling rate were 100 $^{\circ}\text{C}/\text{min}$ and 1000 $^{\circ}\text{C}/\text{min}$, respectively and the holding time was 60 min.

The morphology of the powders, the green samples and the sintered samples was investigated by Scanning electron microscopy (SEM) using a C. Zeiss EVO MA 10. and a Zeiss Crossbeam 540 LA-FIB SEM (Zeiss, Oberkochen, Germany). For the determination of APS values, an analysis of the SEM pictures was conducted; five SEM pictures representing different regions of the initial as well as the milled powder were analyzed, and the particle size ($n = 100$) was measured through the use of Image J 1.47 software [34].

The density of the samples in both green and sintered state was determined by measuring the weight and the dimensions of the samples. The microhardness (HV0.025) of the initial and milled powders was measured by an Instron Wilson Tukon 2100 B (Norwood, MA, USA). The hardness of the green and sintered samples was measured with the Brinell method (HB2.5/62.5) on a Wolpert UH930 machine (Illinois Tool Works Inc. Shanghai, China). Compression tests were carried out in order to determine yield, compression strength and the compression strain. These tests were conducted with Instron 5982 type (Norwood, MA, USA) universal material testing equipment, using a crosshead speed of 3 mm/min.

3. Results and Discussion

3.1. Morphological Analysis

The initial powder has a sponge-like structure with a high specific surface and lots of cavities (Figure 2a). Based on the SEM measurements, the average particle size (APS) of the initial powders was about 180 μm . After ball milling for 20 h, the particles' size and morphology changed to very fine and flake-like with 3 μm APS (Figure 3b). By conducting a wet chemical analysis (ICP-OES Varian 720 ES, Palo Alto, CA, USA) (Table 2), the chemical composition of the initial powder was assessed and compared to the milled powders. Table 2 shows the results. It can be concluded that the composition of the initial and the milled powder slightly differs due to contamination derived from the milling equipment. The amount of contaminant elements has increased due to the long-term high-energy milling, which was, however, an inevitable phenomenon. If we consider that the maximum milled content of the produced sample is 10 wt.%, this impurity overall is

not significant (max. 0.5 wt.%). Moreover, due to the applied rapid and low-energy mixing, the contamination level is not further increased.

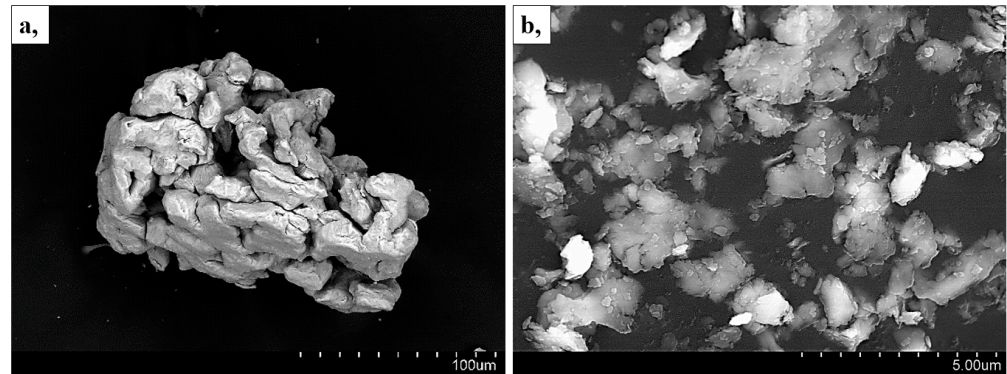


Figure 2. (a,b) Show the morphology of the initial and the milled Ti powders, respectively.

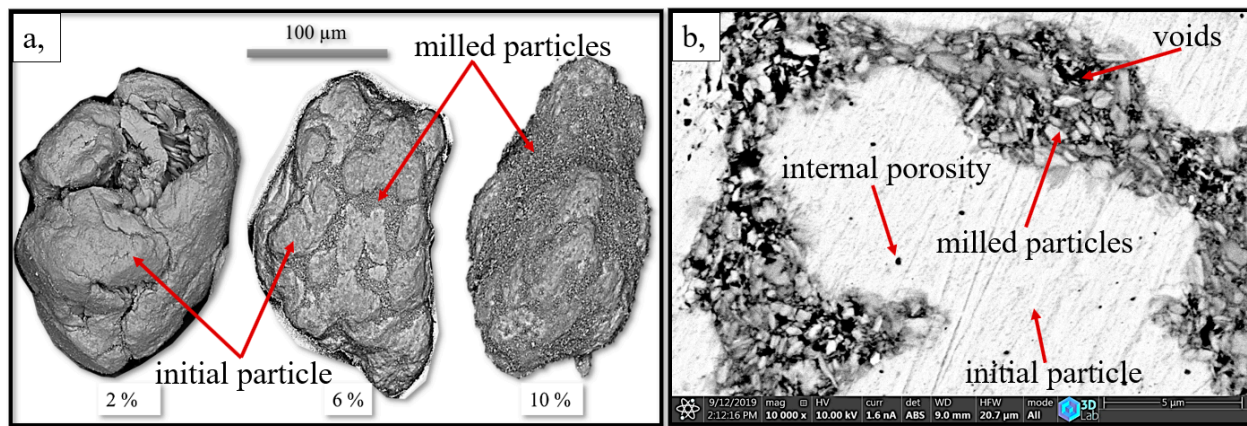


Figure 3. (a) Morphology of the typical particles after mixing the initial powder with 2 wt.%, 6 wt.% and 10 wt.% milled powder; (b) typical SEM images of the green sample which contain 10 wt.% milled powder.

Table 2. Chemical composition of initial and milled Ti powder (wt.%).

Elements	Al	Cr	Cu	Fe	Mn	Ni	Si	Ti
Initial powder	0.0615	0.0015	0.0027	0.0408	0.0003	0.0032	0.365	99.525
Milled powder	0.9701	0.04624	0.0050	1.22	<0.0037	0.0058	1.97	94.473

Due to the intensive plastic deformation caused by high-energy ball milling, not only the particle size, but also the crystallite size, as determined by X-ray diffraction (XRD), was decreased from 180 nm to 4 nm. This value was determined in previous research [35].

The microhardness of the milled powder shows a four-fold increase compared to the initial powder, namely from 200 to 800 HV0.025. During the mixing, these hard and fine particles were trapped within the soft and big initial particles, as can be seen in Figure 4a, wherein different amounts of milled powder content have been considered (2, 6 and 10 wt.%).

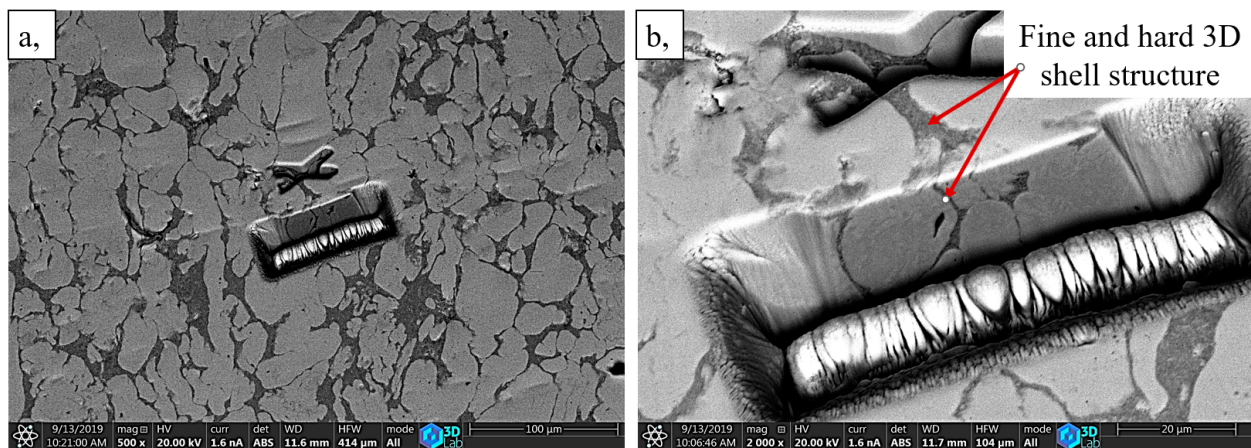


Figure 4. (a,b) SEM images of the samples containing 10 wt.% milled powder after sintering at 850 °C, 1 h at different magnifications.

Based on the SEM images (Figure 3a), it is evident that during the mixing process, the fine, milled powder fills out the pores of the large Ti spongy particles first; afterwards, the surface becomes covered with the fine Ti particles. This structure is visible in the cross-section of the green sample (Figure 3b). Some pores can be seen on Figure 3b, which are mainly closed porosity inside the coarse unmilled particles or voids inside the fine grain shell structure. Figure 4 shows SEM images of a sintered sample with 10 wt.% of ball-milled powders at different magnifications. This sample was sintered at 850 °C for 1 h. The images display both at low and high magnification that the dual-scale structure was not altered during the applied sintering process. The fine milled particles formed a 3D shell structure around the coarse unmilled grains. The thickness of this boundary layer is not constant. It varies between ~1 and ~20 μm. This is a consequence of the different sized voids of the spongy initial powder. However, the APS value of the initial powders was 180 μm, while the size of the coarse grains covered with the fine shell layer was less than ~100 μm in the case of the sintered sample. This means that during the mixing process, the fine particles managed to fill in not just the surface cavities but also the internal ones. The investigated surface has two incisions made by plasma ablation. The aim of these incisions was to prove that this dual-scale structure is truly a 3D structure.

3.2. Density Analysis

Figure 5 shows the effect of the added milled fine powder on the relative density of different green and sintered samples. Based on the density measurements, the milled powder has a notable effect on the properties of the samples. Due to the applied high compacting force (1600 MPa), the relative density of the green sample, which does not contain any milled titanium, was determined to be around ~97.5%. Due to the powder production, the ~2.5% porosity was typically closed porosity. The high green density is beneficial to obtaining high sintered density and high mechanical properties. Robertson et al. applied the same load (1600 MPa) during the cold pressing of Ti6Al4V powder, and the measured green density was ~95% [36]. Raynova et al. has investigated the effect of the green density (65.6% to 96.5%) on the sintered density in the case of HDH Cp-Ti powder. After sintering, the density of the sample with the highest green density remained the highest (~97%) [24]. In our research, the results showed the same tendency. The density of the green sample, which does not contain any milled titanium, practically does not change during the sintering temperatures. As it can be seen in Figure 5, the green density values were decreased by increasing the fraction of the milled powder. This is due to the fact that porosities take place between the hard particles of the milled fraction (Figure 3b) which add to the micro porosities inside the powder particles. Moreover, the increase in sintering temperature resulted in an exponential increase in density. This is due to the fact

that the specific interface increases with fine grains, which increases the driving force of sintering [37].

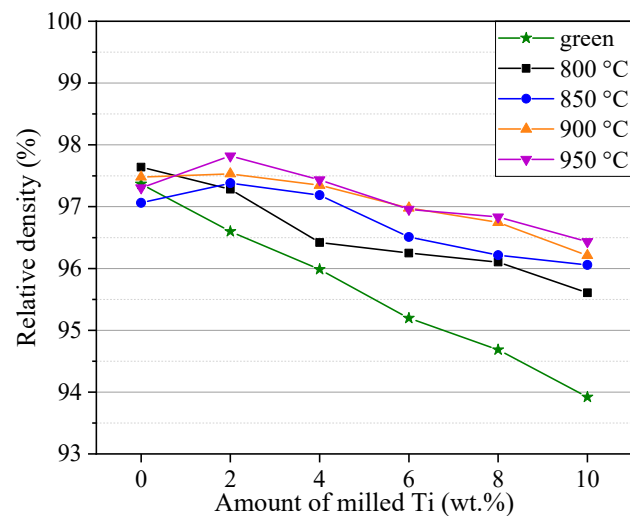


Figure 5. Relative density of the samples containing different amount of milled Ti.

Despite the applied low sintering temperature and short sintering time, the sintered density of the produced samples was found to be similar or better, compared with those observed in the literature (Table 3). As the values show, the applied processing parameters have a significant effect on the density.

Table 3. Density values of different titanium and Ti alloy sintered at different conditions.

Powder Type	D50 (μm)	Green Density (%)	Sintered Density (%)	Sintering Temperature ($^{\circ}\text{C}$)	Sintering Time (min)
Current research Ti sponge+6% milled Ti	180	95.2	97	900	60
Ti irregular [38]	30	60	95.8	1250	120
Ti sphere [39]	23	67	89.6	1000	120
Ti sphere [37]	74	52	63.5	850	60
Ti irregular [40]	18	68	82.5	1250	60
Ti6Al4V sphere [41]	35	65	97.5	1400	120
Ti6Al4V irregular [42]	39	69	93.5	1300	120

3.3. Hardness Results

The hardness of the green samples was not influenced by the amount of milled Ti content, simply due to the fact that these samples do not present an adequate integrity in the green state (Figure 6). The hardness of all sintered samples, which had no milled powder ranges, was between 180 and 210 HB. This hardness value corresponds to the standard hardness of the Cp-Ti grade 2 (200 HB). However, the amount of milled powder had a significant effect on the hardness. The hardness increased with an increase of the milled Ti content. The highest hardness was obtained at a sintering temperature of 850 $^{\circ}\text{C}$. Higher temperatures resulted in a slight decrease in hardness. This can be explained by the recrystallization or coarsening process, which occurs above 850 $^{\circ}\text{C}$, resulting in grain growth and a decrease in hardness or strength [43]. The sample that contained 10 wt.% milled powder showed the highest hardness (350 HB) sintered at 850 $^{\circ}\text{C}$. This value is equal to the hardness of the Ti6Al4V [10].

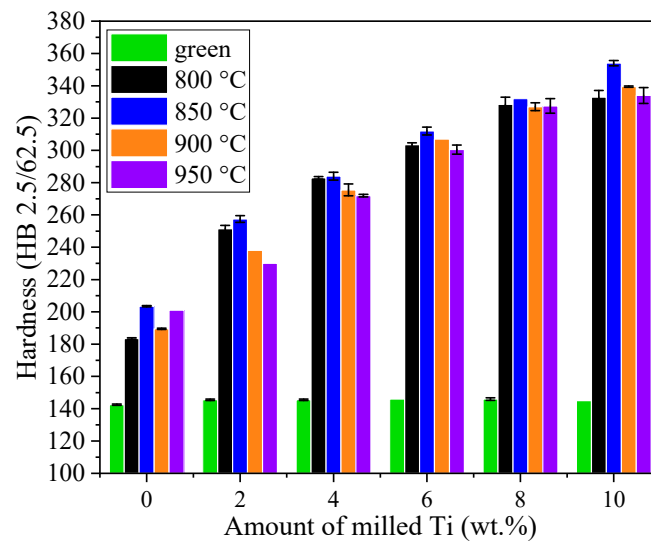


Figure 6. Hardness of the samples with different amounts of milled Ti.

3.4. Compression Test Results

The yield strength is probably the most important mechanical property of the material. This value determines the maximal mechanical loads that the material can withstand without deformation. This value is also influenced by the direction of the load. There are some studies which applied both the tensile and compression test on the sintered Ti samples. Schulze et al. determined the YS of SLM-produced Ti-42Nb alloy on tensile and compression specimen. The YS was 674 MPa upon tensile test and 831 MPa upon compression test, respectively [26]. Raghavendra et al. compared the tensile and compressive properties of additively manufactured (SLM) Ti6Al4V porous samples. The ultimate tensile strength was lower than compressive strength by an average value of 100 MPa [44]. We have to account for the fact that the PM samples have a significant number of defects, e.g., porosities. Generally, the sensitivity of the tensile test properties on the presence of defects is much higher than in the case of a compression test. Figure 7 shows the measured engineering stress–engineering strain curves of samples sintered at 800 °C, determined by compression test.

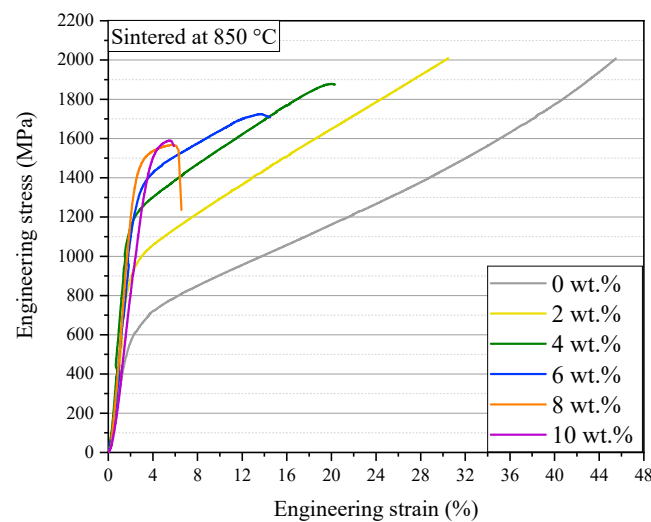


Figure 7. Stress–strain curves of the samples sintered at 850 °C with different milled Ti content.

Strength values (YS, compressive strength) determined on the measured curves show the same tendency as the hardness results. The samples without milled Ti content had an average YS (500–640 MPa). On the other hand, for the samples with an increased milled

Ti content, the YS increased proportionally (Figure 8). The highest strength values in most cases belong to the samples sintered at 850 °C. Regarding the strain values of the compression tests, it can be concluded that increasing the milled fraction decreases the deformability of the material.

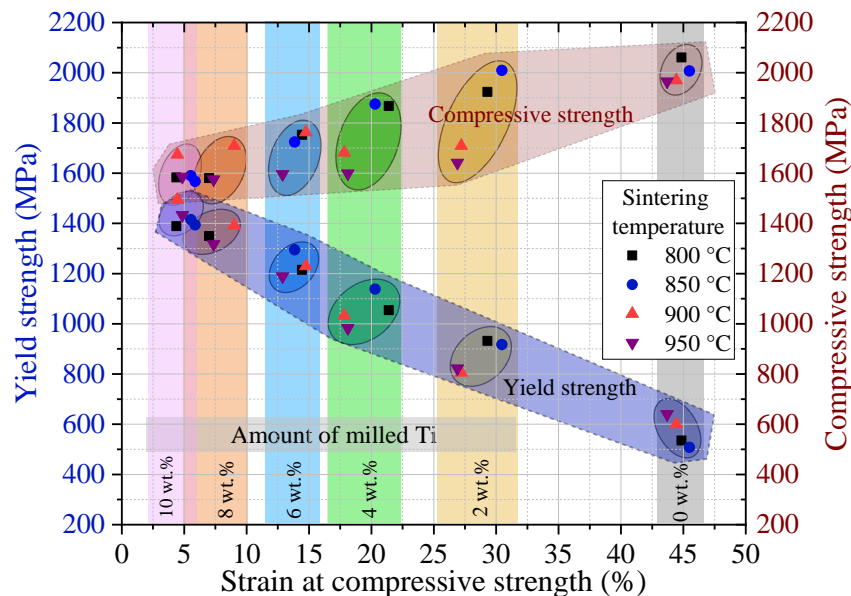


Figure 8. Strength and strain values of the measured samples.

The samples with 8 wt.% milled Ti presented a reduced formability around 5%, meaning that the material is too brittle for engineering applications. Comparing the measured YS values with data from the literature, it can be stated that the sample that has 6 wt.% milled powder shows a higher YS than the wrought Ti6Al4V (Table 4).

Table 4. Mechanical properties of titanium alloys fabricated by various processing technologies. (compressive YS; ultimate compressive strength, plastic strain to maximum compressive stress).

Material	Processing Method	Yield Strength (MPa)	Compressive Strength (MPa)	Strain at Maximum Stress (%)	Source
Ti-6% milled Ti (850 °C)	Press and Sinter	1295	1724	14	Current Research
CP-Ti	ECAP	700	900	35	[43]
CP-Ti	SLM	560	1136	51	[45]
Ti6Al4V	Annealed	1000	1300	10	[46]
Ti6Al4V	Wrought	1200	1400	20	[47]

4. Summary

In this study, different mixtures of coarse (180 μm APS) and fine (3 μm APS) Cp-Ti 2 powders were used for the production of a pure Ti material. The fine powder was milled from the initial coarse powder by use of high-energy planetary ball milling.

During the mixing process, the finely milled flakes were trapped and filled the pores of the coarse spongy particles and covered their surface. Cylindrical samples were produced from the different mixtures via uniaxial cold pressing. In order to minimize the porosity of the green samples, the various feedstock mixtures (0–10 wt.% fine powder) were cold-pressed at an extremely high uniaxial pressure (1.6 GPa).

The relative density of the cold-pressed samples varied between 97% and 94% depending on the proportion of fine particles. These density values are particularly high compared to literature data (52–69%), which is due to the good deformability of the rough and soft titanium sponge, which accounts for 90–98 wt.% of the produced samples.

This high green density allows the use of low-temperature and rapid sintering (800–950 °C, 60 min in 6.0 argon atmosphere), as long-distance atomic movement is not required during the densification process. The relative density of the sintered samples varied between 95.6% and 97.8%, which is comparable with corresponding results from the literature (93.5 to 97.5%).

Due to the applied sintering conditions, the coarsening of the initial dual-scale structure has not occurred, and the comparable hardness (max. 350 HB) and compressive properties (max. 1492 MPa YS) of the Ti6Al4V alloy were measured. The production parameters of the optimal strength–strain version of the alloy were 6 wt.% amount of milled Ti and 850 °C sintering temperature. It is possible that the inhomogeneous microstructure with large and fine features could contribute to differences between the compression and tensile test results. The presence of these features could cause variations in stress distribution and lead to localized deformation or failure during testing. Additionally, the presence of large features could affect the sample geometry and cause stress concentrations, which could also influence the test results. This constitutes a matter for further research.

In summary, a quasi-pure Ti material was produced with comparable to the Ti6Al4V alloy properties by use of a production method which is cheaper, more energy efficient, and consequently more environmentally friendly than conventional techniques. The latter factor is due to the low temperature and the rapid sintering applied. Moreover, the produced Ti parts are more easily recyclable due to the absence of alloying elements. The latter advantages make our material a potential candidate for consideration in aerospace applications requiring high strength, as the above characteristics contribute to the goals and aims of sustainable and circular aviation [48,49].

A complete LCA and LCC analysis of the production route could be the subject of further research in order to quantify the exact environmental and cost gains of the whole process compared to conventional production processes. Moreover, further research will be needed, including tensile and fatigue tests, to address the complete mechanical characterization of novel materials. The measuring of the effect of contamination by, for example, iron or oxygen should be part of a future research. Finally, further optimization of the production process will probably boost and lead to more uniform properties.

Author Contributions: Conceptualization, T.M., Z.G. and D.M.; methodology, T.M.; software, T.M.; validation, T.M. and D.P.; formal analysis, D.P. and G.G.; investigation, T.M.; resources, Z.G. and G.G.; data curation, T.M.; writing—original draft preparation, T.M., D.M. and D.P.; writing—review and editing, T.M., D.M., D.P. and Z.G.; visualization, T.M. and Z.G.; supervision, Z.G.; project administration, G.G. All authors have read and agreed to the published version of the manuscript.

Funding: The research was supported by the UMA³ project, funded by the European Union's Horizon 2020 research and innovation program under grant agreement No. 952463.

Conflicts of Interest: The authors declare no conflict of interest.

References

1. Kulkarni, K.G.; Bhattacharya, N. Use of titanium and its alloy in aerospace and aircraft industries. *Int. J. Creat. Res. Thoughts* **2020**, *8*, 1383–1396.
2. Gholizadeh, S. Impact behaviours and Non-Destructive Testing (NDT) methods in Carbon Fiber Composites in Aerospace Industry: A Review. *Authorea Prepr.* **2022**. [[CrossRef](#)]
3. Liu, S.; Shin, Y.C. Additive manufacturing of Ti6Al4V alloy: A review. *Mater. Des.* **2019**, *164*, 107552. [[CrossRef](#)]
4. Williams, J.C.; Boyer, R.R. Opportunities and Issues in the Application of Titanium Alloys for Aerospace Components. *Metals* **2020**, *10*, 705. [[CrossRef](#)]
5. Inagaki, I.; Takechi, T.; Ariyasu, Y.S. Application and Features of Titanium for the Aerospace Industry. *Nippon. Steel Sumitomo Met. Tech. Rep.* **2014**, *106*, 22–27.
6. Niinomi, M.; Kagami, K. Recent topics of titanium research and development in Japan. In Proceedings of the 13th World Conference on Titanium, San Diego, CA, USA, 16–20 August 2016.
7. Zang, M.C.; Niu, H.Z.; Yu, J.S.; Zhang, H.R.; Zhang, T.B.; Zhang, D.L. Cryogenic tensile properties and deformation behavior of a fine-grained near alpha titanium alloy with an equiaxed microstructure. *Mater. Sci. Eng.* **2022**, *840*, 142952. [[CrossRef](#)]

8. Markatos, D.N.; Pantelakis, S.G. Assessment of the Impact of Material Selection on Aviation Sustainability, from a Circular Economy Perspective. *Aerospace* **2022**, *9*, 52. [CrossRef]
9. Available online: https://www.aubertduval.com/wp-media/uploads/2022/07/Titane_brochure_202207.pdf (accessed on 10 February 2023).
10. Frohes, F.H. *Titanium Physical Metallurgy, Processing, and Applications*; ASM International: Almere, The Netherlands, 2015.
11. Oleksik, V.; Trzpiecinski, T.; Szpunar, M.; Chodola, L.; Ficek, D.; Szczesny, I. Single-Point Incremental Forming of Titanium and Titanium Alloy Sheets. *Materials* **2021**, *14*, 6372. [CrossRef]
12. OnlineMetals.com. Available online: <https://www.onlinemetals.com> (accessed on 5 February 2023).
13. Fang, Z.Z.; Paramore, J.D.; Sun, P.; Chandran, K.S.R.; Zhang, Y.; Xia, Y.; Cao, F.; Koopman, M.; Free, M. Powder metallurgy of titanium—Past, present, and future. *Int. Mater. Rev.* **2017**, *63*, 407–459. [CrossRef]
14. Zwitter, T.M.; Nash, P.; Xu, X.; Johnson, C. Energy Efficient Press and Sinter of Titanium Powder for Low-Cost Components in Vehicle Applications Final Scientific Report. 2011. Available online: <https://www.osti.gov/servlets/purl/1020890> (accessed on 10 February 2023).
15. Henriques, V.A.R. Titanium production for aerospace applications. *J. Aerosp. Technol. Manag.* **2009**, *1*, 7–17. [CrossRef]
16. Abkowitz, S.M.; Abkowitz, S.; Fisher, H. Breakthrough claimed for titanium PM. *Met. Powder Rep.* **2011**, *66*, 16–21. [CrossRef]
17. Araci, K.; Mangabhai, D.; Akhtar, K. Production of titanium by the Armstrong Process. In *Titanium Powder Metallurgy, Science, Technology and Applications*; Elsevier: Amsterdam, The Netherlands, 2015; pp. 149–162.
18. Allied Titanium, Inc. Available online: <https://www.alliedtitanium.com/> (accessed on 5 February 2023).
19. Duriagina, Z.A.; Lemishka, I.A.; Trostianchyn, A.M.; Kulyk, V.V.; Shvachki, S.G.; Tepla, T.L.; Pleshakov, E.I.; Kosbasyuk, T.M. The effect of morphology and particle-size distribution of VT20 Titanium alloy powders on the mechanical properties of deposited coatings. *Powder Metall. Met. Ceram.* **2019**, *57*, 697–702. [CrossRef]
20. Chen, B.; Shen, J.; Ye, x.; Umeda, J.; Kondoh, K. Advanced mechanical properties of powder metallurgy commercially pure titanium with a high oxygen concentration. *J. Mater. Res.* **2017**, *32*, 19. [CrossRef]
21. Dong, S.; Ma, G.; Lei, P.; Cheng, T.; Savvakina, D.; Ivasishin, O. Comparative study on the densification process of different titanium powders. *Adv. Powder Technol.* **2021**, *32*, 2300–2310. [CrossRef]
22. Xu, X.; Zheng, Y.; Liang, H.; Yang, M.; Zhao, Y.; Zhou, W. Influence of sintering parameters on the grain growth and mechanical properties of Ti(C,N)-based cermets prepared via mechanical activation and in-situ carbothermal reduction. *Mater. Today Commun.* **2022**, *33*, 104667. [CrossRef]
23. Wang, H.; Fang, Z.Z.; Sun, P. A critical review of mechanical properties of powder metallurgy titanium. *Int. J. Powder Metall.* **2010**, *46*, 45–57.
24. Raynova, S.; Collas, Y.; Yang, F.; Bolzoni, L. Advancement in the Pressureless Sintering of CP Titanium Using High-Frequency Induction Heating. *Metall. Mater. Trans. A* **2019**, *50*, 4732–4742. [CrossRef]
25. Sidambe, A.T. Biocompatibility of Advanced Manufactured Titanium Implants A Review. *Materials* **2014**, *7*, 8168–8188. [CrossRef]
26. Schulze, C.; Weinmann, M.; Schweigel, C.; Kessler, O.; Bader, R. Mechanical Properties of a Newly Additive Manufactured Implant Material Based on Ti-42Nb. *Materials* **2018**, *11*, 124. [CrossRef]
27. Chen, B.Y.; Hwang, K.S.; Ng, K.L. Effect of cooling process on the phase formation and mechanical properties of sintered Ti–Fe alloys. *Mater. Sci. Eng. A* **2011**, *528*, 4556–4563. [CrossRef]
28. Jeong, H.W.; Kim, S.J.; Hyun, Y.T.; Lee, Y.T. Densification and Compressive Strength of In-situ Processed Ti/TiB Composites by Powder Metallurgy. *Met. Mater. Int.* **2002**, *8*, 25–35. [CrossRef]
29. Tellkamp, V.L.; Melmed, A.; Lavernia, E.J. Mechanical Behavior and Microstructure of a Thermally Stable Bulk Nanostructured Al Alloy. *Metall. Mater. Trans. A* **2001**, *32*, 2335–2343. [CrossRef]
30. Okulov, I.V.; Kühn, U.; Marr, T.; Freudenberger, J.; Schultz, L.; Oertel, C.G.; Skrotzki, W.; Eckert, J. Deformation and fracture behavior of composite structured Ti-Nb-Al-Co(-Ni) alloys. *Appl. Phys. Lett.* **2015**, *104*, 071905. [CrossRef]
31. Sun, Y.; Luo, G.; Zhang, J.; Chen, J.; Wang, G.; Shen, Q.; Zhang, L. Microstructure, mechanical properties and reinforcement mechanism of dual-scale TC4 titanium alloy prepared by cryomilling and plasma activated sintering. *Mater. Sci. Eng. A* **2018**, *736*, 120–129. [CrossRef]
32. Li, Z.; Dong, A.; Xing, H.; Xu, H.; Du, D.; Zhang, T.; She, H.; Wang, D.; Zhu, G.; Sun, B. Microstructure and mechanical properties of bimodal Ti-Bi alloys fabricated by mechanical alloying and spark plasma sintering for biomedical applications. *Mater. Charact.* **2020**, *161*, 110134. [CrossRef]
33. Attar, H.; Ehtemam-Haghighi, S.; Kent, D.; Dargusch, M.S. Recent developments and opportunities in additive manufacturing of titanium-based matrix composites: A review. *Int. J. Mach. Tools Manuf.* **2018**, *133*, 85–102. [CrossRef]
34. Rasband, W.S. *ImageJ*; U.S. National Institutes of Health: Bethesda, MD, USA, 1997–2018. Available online: <https://imagej.nih.gov/ij/> (accessed on 5 February 2023).
35. Angel, D.A.; Miko, T.; Kristaly, F.; Benke, M.; Gacsi, Z. Development of TiB and nanocrystalline Ti-reinforced novel hybrid Ti nanocomposite produced by powder metallurgy. *J. Mater. Sci.* **2022**, *57*, 4130–4144. [CrossRef]
36. Robertson, I.M.; Schaffer, G.B. Review of densification of titanium based powder systems in press and sinter processing. *Powder Metall.* **2010**, *53*, 146–162. [CrossRef]
37. German, R.M. Titanium sintering science: A review of atomic events during densification. *Int. J. Refract. Met. Hard Mater.* **2020**, *89*, 105214. [CrossRef]

38. Cai, Y.X.; Chang, Q.; Ding, Y. Research of injection molding titanium parts. *Powder Metall. Tech.* **2005**, *23*, 449–455.
39. Ieki, T.; Katoh, K.; Matsumoto, A.; Masui, T.; Andoh, K. Tensile properties of sintered Ti compacts by metal injection Molding process. *J. Jap. Soc. Powder Metall.* **1997**, *44*, 448–452. [[CrossRef](#)]
40. Panigrahi, B.B.; Godkhindi, M.M.; Das, K.; Mukunda, P.G. Ramakrishnan, P. Sintering kinetics of micrometric titanium powder. *Mater. Sci. Eng.* **2005**, *A396*, 255–262. [[CrossRef](#)]
41. Ferri, O.M.; Ebel, T.; Bormann, R. The influence of small boron addition on the microstructure and mechanical properties of Ti-6Al-4V fabricated by metal injection moulding. *Adv. Eng. Mater.* **2011**, *13*, 436–447. [[CrossRef](#)]
42. Bolzoni, L.; Ruiz-Navas, E.M.; Gordo, E. Influence of sintering parameters on the properties of powder metallurgy Ti-3Al-2.5V alloy. *Mater. Charact.* **2013**, *84*, 48–58. [[CrossRef](#)]
43. Long, F.W.; Jiang, Q.W.; Xiao, L.; Li, X.W. Compressive Deformation Behaviors of Coarse- and Ultrafine-Grained Pure Titanium at Different Temperatures: A Comparative Study. *Mater. Trans.* **2011**, *52*, 1617–1622. [[CrossRef](#)]
44. Raghavendra, S.; Molinari, A.; Fontanari, V.; Luchin, V.; Zappini, G.; Benedetti, M.; Johansson, F.; Klarin, J. Tensile and compression properties of variously arranged porous Ti-6Al-4V additively manufactured structures via SLM. *Procedia Struct. Integr.* **2018**, *13*, 149–154. [[CrossRef](#)]
45. Attar, H.; Bönisch, M.; Calin, M.; Zhang, L.C.; Scudino, S.; Eckert, J. Selective laser melting of in situ titanium–titanium boride composites: Processing, microstructure and mechanical properties. *Acta Mater.* **2014**, *76*, 13–22. [[CrossRef](#)]
46. Srinivasan, K.; Venugopal, P. Compression Testing of Ti-6Al-4V in the Temperature Range of 303–873 K. *Mater. Manuf. Process.* **2008**, *23*, 342–346. [[CrossRef](#)]
47. Fadida, R.; Rittel, D.; Shirizly, A. Dynamic Mechanical Behavior of Additively Manufactured Ti6Al4V with Controlled Voids. *J. Appl. Mech.* **2015**, *82*, 041004. [[CrossRef](#)]
48. European Commission. *Flightpath 2050, Europe's Vision for Aviation*; Report of the High Level Group on Aviation Research, Directorate-General for Research and Innovation, Directorate General for Mobility and Transport; European Commission: Brussels, Belgium, 2011; p. 28.
49. Communication from the Commission to the European Parliament, the European Council, the European Economic and Social Committee and the Committee of the Regions the European Green Deal com/2019/640 Final. Available online: <https://eur-lex.europa.eu/legal-content/EN/TXT/?uri=COM%3A2019%3A640%3AFIN> (accessed on 13 February 2023).

Disclaimer/Publisher's Note: The statements, opinions and data contained in all publications are solely those of the individual author(s) and contributor(s) and not of MDPI and/or the editor(s). MDPI and/or the editor(s) disclaim responsibility for any injury to people or property resulting from any ideas, methods, instructions or products referred to in the content.